Electronic Supplementary Material (ESI) for Journal of Materials Chemistry A.

Supporting Information

Large-scale Cascade Cooling Performance Evaluation of Adsorbent/Water Working Pairs by Integrated Mathematical Modelling and Machine Learning

Zhilu Liu [a], Wei Li [b], Shanshan Cai [a], Zhengkai Tu [a], Xiaobing Luo [a] and Song Li [a,*]

[a] School of Energy and Power Engineering, Huazhong University of Science and Technology, Wuhan 430074, China.

[b] Energy & Electricity Research Center, Jinan University, Zhuhai 519070, China.

* Corresponding author email: songli@hust.edu.cn.

Table of Contents

S1. Supplementary tables in an Excel file

Table S1. The number of adsorbents with reported structural properties in the literature

Species	Adsorbents No.	Adsorbents No. with Reported Structural Properties		
		S_a (m^2/g)	V_a (cm^3/g)	D_p (Å)
Carbon materials (Carb)	37	31	33	17
COFs (C)	57	55	31	33
MOFs (M)	176	107	78	111
POPs (P)	30	28	26	12
Zeolites (Z)	11	7	7	4
Sum	311	228	175	187

Table S2. Source of literature corresponding to 311 adsorbents studied in this work.

Table S3. Fitting parameters of 311 water adsorption isotherms using universal adsorption isotherm model.

Table S4. Structural characteristics of adsorbents collected from the literature.

Table S5. Adsorption properties of adsorbents in the high-temperature stage (HS) and low-temperature stage (LS).

Table S6. Cooling performance of adsorbent/water working pairs in cascaded adsorption chillers (two-stage, TS).

S2. Computation details of cooling performance based on the ideal isosteric diagram of cACs

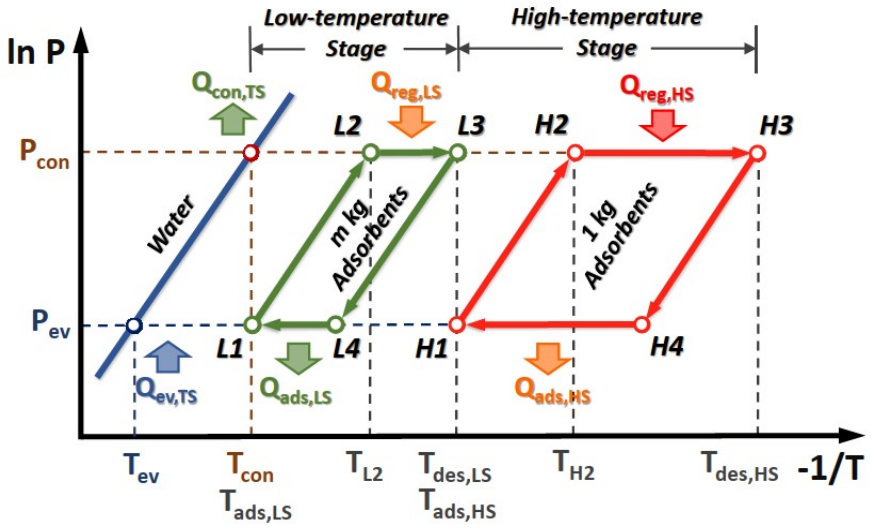

Figure S1. The ideal isosteric diagram of cascaded adsorption chillers (cACs) consists of the low-temperature stage (LS, L1-L4) and high-temperature stage (HS, H1-H4). Q represents the transferred heat by adsorbent/water working pairs.

Under given operational conditions in Table 3, the working capacity (ΔW) equals the difference of water uptake between adsorption and desorption obtained from predicted isotherms by universal adsorption isotherm model (UAIM) as described in Eq. S1.[1]

$$W = \sum_{i=1}^{n} \alpha_i \left\{ \frac{\left(\frac{P}{P_0} \exp\left(\frac{\varepsilon_i}{RT} \right) \right)^{\frac{RT}{m_i}}}{1 + \left(\frac{P}{P_0} \exp\left(\frac{\varepsilon_i}{RT} \right) \right)^{\frac{RT}{m_i}}} \right\}_i \quad \text{(Eq. S1)}$$

W is the water equilibrium uptake, P and T represent the equilibrium pressure and temperature, and P_0 is the saturation pressure of water, R is the ideal gas constant. Additionally, α_i, ε_i, m_i and n are fitting parameters that are determined by the characteristic of adsorption isotherms given in Table S1.

The cascaded adsorption chillers (cACs) consist of the low-temperature stage (LS) and high-temperature stage (HS). In HS and LS, the ΔW (unit: kg/kg) can be obtained by Eq .S2 and Eq. S3.

$$\Delta W_{HS} = \Delta W_{max,HS} - \Delta W_{mmi,HS} = W_{HS}\left(T_{ads,HS}, P_{ev}\right) - W_{HS}\left(T_{des,HS}, P_{con}\right) \quad \text{(Eq. S2)}$$

$$\Delta W_{LS} = \Delta W_{max,LS} - \Delta W_{mmi,LS} = W_{LS}\left(T_{ads,LS}, P_{ev}\right) - W_{LS}\left(T_{des,LS}, P_{con}\right) \quad \text{(Eq. S3)}$$

The cooling performance including coefficient of performance for cooling (COP_C) and specific cooling effects (SCE) of the single-stage can be calculated based on basic thermodynamic cycle under given working conditions. [2]

$$SCE_{HS} = Q'_{ev,HS} = \Delta W_{HS}\left[\Delta_{vap}H\left(T_{ev}\right) - C_p^{wf}\left(T_{con} - T_{ev}\right)\right] \quad \text{(Eq. S4)}$$

$$SCE_{LS} = Q'_{ev,LS} = \Delta W_{LS}\left[\Delta_{vap}H\left(T_{ev}\right) - C_p^{wf}\left(T_{con} - T_{ev}\right)\right] \quad \text{(Eq. S5)}$$

$$\mathrm{COP_{C,HS}} = \frac{Q'_{\mathrm{ev,HS}}}{Q'_{\mathrm{reg,HS}}} = \frac{\Delta W_{\mathrm{HS}}\left[\Delta_{\mathrm{vap}}H\left(T_{\mathrm{ev}}\right) - C_{\mathrm{p}}^{\mathrm{wf}}\left(T_{\mathrm{con}} - T_{\mathrm{ev}}\right)\right]}{C_{\mathrm{p}}^{\mathrm{ad}}\left(T_{\mathrm{des,HS}} - T_{\mathrm{ads,HS}}\right) + C_{\mathrm{p}}^{\mathrm{wf}}\left[W_{\mathrm{HS}}\left(T_{\mathrm{ads,HS}}, P_{\mathrm{ev}}\right)\left(T_{\mathrm{H2}} - T_{\mathrm{ads,HS}}\right) + \int_{T_{\mathrm{H2}}}^{T_{\mathrm{des,HS}}} W_{\mathrm{HS}}\left(T\right)\mathrm{d}T\right] - \Delta W_{\mathrm{HS}}\Delta_{\mathrm{ads}}H_{\mathrm{ave,HS}}} \quad \text{(Eq. S6)}$$

$$\mathrm{COP_{C,LS}} = \frac{Q'_{\mathrm{ev,LS}}}{Q'_{\mathrm{reg,LS}}} = \frac{\Delta W_{\mathrm{LS}}\left[\Delta_{\mathrm{vap}}H\left(T_{\mathrm{ev}}\right) - C_{\mathrm{p}}^{\mathrm{wf}}\left(T_{\mathrm{con}} - T_{\mathrm{ev}}\right)\right]}{C_{\mathrm{p}}^{\mathrm{ad}}\left(T_{\mathrm{des,LS}} - T_{\mathrm{ads,LS}}\right) + C_{\mathrm{p}}^{\mathrm{wf}}\left[W_{\mathrm{LS}}\left(T_{\mathrm{ads,LS}}, P_{\mathrm{ev}}\right)\left(T_{\mathrm{L2}} - T_{\mathrm{ads,LS}}\right) + \int_{T_{\mathrm{L2}}}^{T_{\mathrm{des,LS}}} W_{\mathrm{LS}}\left(T\right)\mathrm{d}T\right] - \Delta W_{\mathrm{LS}}\Delta_{\mathrm{ads}}H_{\mathrm{ave,LS}}} \quad \text{(Eq. S7)}$$

Here, Q'_{ev} represents the transferred heat in the evaporator by water working capacity of 1 kg adsorbents, and Q'_{reg} represents the regeneration energy required for 1 kg adsorbents. In these formulas, the specific heat capacity of the adsorbent (C_p^{ad})and working fluid (C_p^{wf}) are considered to be constant, they are 1 (reasonable value for a variety of adsorbents) [3] and 4.2 kJ/(kg·K) (for water). Additionally, the vaporization enthalpy ($\Delta_{vap}H$, unit is kJ/kg) of water that is a function of temperature.

$$\Delta_{\mathrm{vap}}H\left(T\right) = -2.51\left(T - 273\right) + 2502 \quad \text{(Eq. S8)}$$

The heat of adsorption ($\Delta_{ads}H$) is calculated using the predicted adsorption isotherms obtained by the universal isotherm adsorption model at varying temperatures according to the Clausius-Clapeyron equation shown in Eq. S9.

$$\Delta_{\mathrm{ads}}H = -\mathrm{R}\frac{\partial\left(\ln p\right)}{\partial\left(1/T\right)} \quad \text{(Eq. S9)}$$

Then the average heat of adsorption ($\Delta_{ads}H_{ave}$) of adsorbents can be estimated as follows:

$$\Delta_{\mathrm{ads}}H_{\mathrm{ave}} = \frac{\int_{W_{\mathrm{min}}}^{W_{\mathrm{max}}} \Delta_{\mathrm{ads}}H\ \mathrm{d}W}{W_{\mathrm{max}} - W_{\mathrm{min}}} \approx \frac{\int_{0}^{W_{\mathrm{sat}}} \Delta_{\mathrm{ads}}H\ \mathrm{d}W}{W_{\mathrm{sat}}} \quad \text{(Eq. S10)}$$

For cACs in Figure S1, in ideal conditions, it is assumed that 1 kg adsorbents were desorbed in HS, and all the heat released from HS was used for complete regeneration of m kg adsorbents in LS. Therefore, m equals to the ratio of $Q'_{reg,HS}$ and $Q'_{reg.,LS}$.

$$m = \frac{Q'_{\mathrm{reg,HS}}}{Q'_{\mathrm{reg,LS}}} = \frac{\int_{T_{\mathrm{ads,HS}}}^{T_{\mathrm{des,HS}}} C_{\mathrm{p}}^{\mathrm{ad}}\left(T\right)\mathrm{d}T + W\left(T_{\mathrm{ads,HS}}, P_{\mathrm{ev}}\right)\int_{T_{\mathrm{ads,HS}}}^{T_{\mathrm{H2}}} C_{\mathrm{p}}^{\mathrm{wf}}\left(T\right)\mathrm{d}T + \int_{T_{\mathrm{H2}}}^{T_{\mathrm{des,HS}}} W\left(T\right)C_{\mathrm{p}}^{\mathrm{wf}}\left(T\right)\mathrm{d}T + \Delta W_{\mathrm{HS}}\Delta_{\mathrm{ads}}H_{\mathrm{HS}}}{\int_{T_{\mathrm{ads,LS}}}^{T_{\mathrm{des,LS}}} C_{\mathrm{p}}^{\mathrm{ad}}\left(T\right)\mathrm{d}T + W\left(T_{\mathrm{ads,LS}}, P_{\mathrm{ev}}\right)\int_{T_{\mathrm{ads,LS}}}^{T_{\mathrm{L2}}} C_{\mathrm{p}}^{\mathrm{wf}}\left(T\right)\mathrm{d}T + \int_{T_{\mathrm{L2}}}^{T_{\mathrm{des,LS}}} W\left(T\right)C_{\mathrm{p}}^{\mathrm{wf}}\left(T\right)\mathrm{d}T + \Delta W_{\mathrm{LS}}\Delta_{\mathrm{ads}}H_{\mathrm{LS}}} \quad \text{(Eq. S11)}$$

Therefore, according to the definition of SCE and COP_C, the SCE in the total system (SCE_{TS}) and COP_C in the total system ($COP_{C,TS}$) can be calculated as follows.

$$\mathrm{SCE_{TS}} = \frac{Q_{\mathrm{ev,TS}}}{1+m} = \frac{Q_{\mathrm{ev,HS}} + Q_{\mathrm{ev,LS}}}{1+m} = \frac{Q'_{\mathrm{ev,HS}} + mQ'_{\mathrm{ev,LS}}}{1+m} = \frac{\mathrm{SCE_{HS}} + m\mathrm{SCE_{LS}}}{1+m} \quad \text{(Eq. S12)}$$

$$\mathrm{COP_{C,TS}} = \frac{Q_{\mathrm{ev,TS}}}{Q_{\mathrm{reg,HS}}} = \frac{Q'_{\mathrm{ev,HS}} + mQ'_{\mathrm{ev,LS}}}{Q'_{\mathrm{reg,HS}}} = \frac{Q'_{\mathrm{ev,HS}} + \frac{Q'_{\mathrm{reg,HS}}}{Q'_{\mathrm{reg,LS}}} \times Q'_{\mathrm{ev,LS}}}{Q'_{\mathrm{reg,HS}}} = \mathrm{COP_{C,HS}} + \mathrm{COP_{C,LS}} \quad \text{(Eq. S13)}$$

Therefore, under given operational conditions, the cooling performance including SCE_{TS} and $COP_{C,TS}$ can be obtained by combining the equations abovementioned.

S3. Cooling performance of adsorbents/water working pairs for cACs

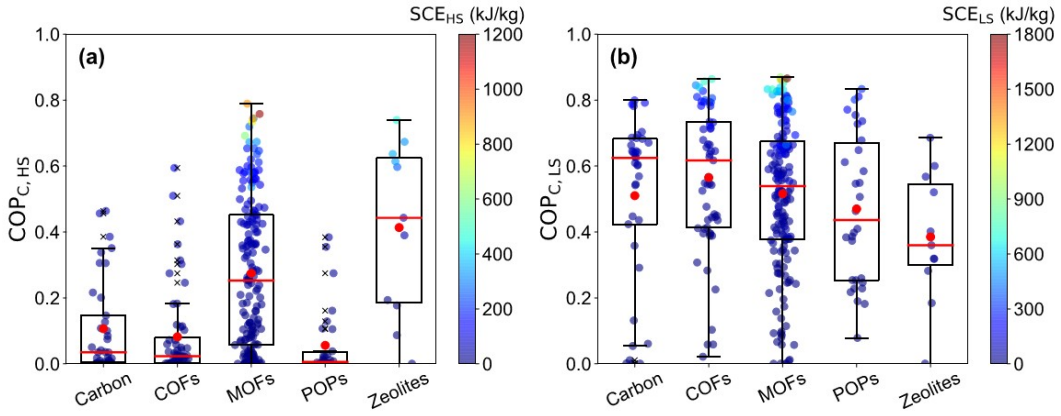

Figure S2. The distribution of different adsorbent species with the varying coefficient of performance for cooling (COP_C) and specific cooling effects (SCE) in (a) high-temperature stage (HS) and (b) low-temperature stage (LS).

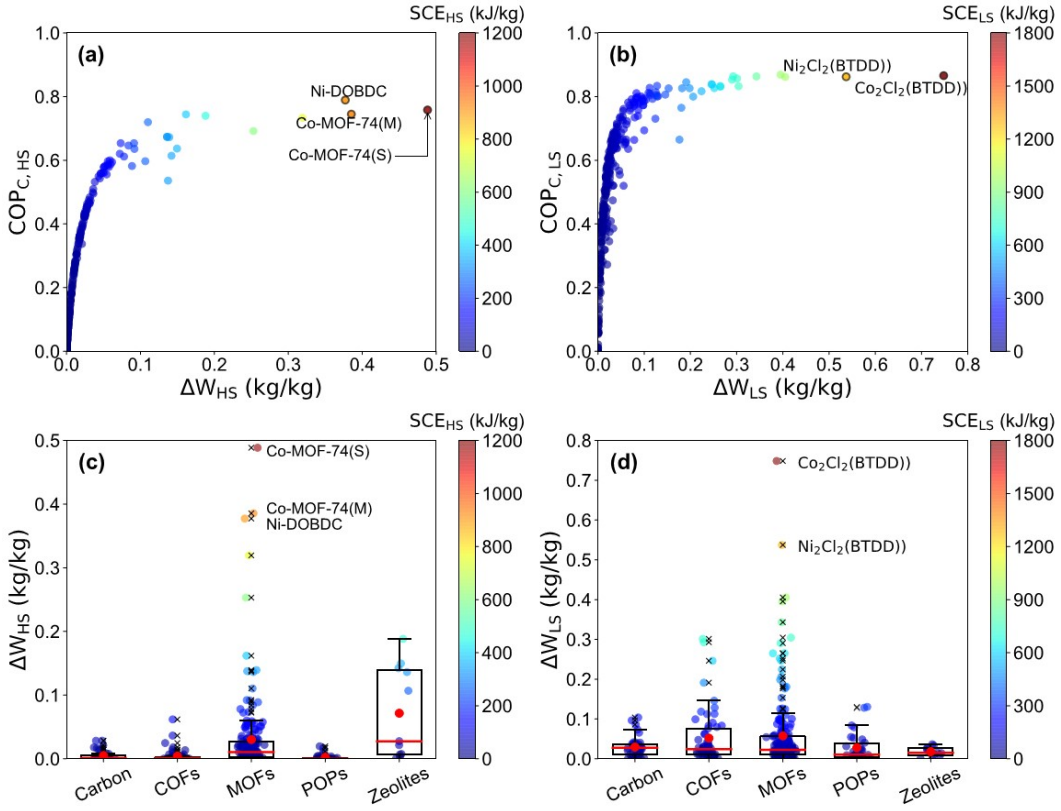

Figure S3. The relationship between the coefficient of performance for cooling (COP_C) and water working capacity (ΔW) in (a) high-temperature stage (HS) and (b) low-temperature stage (LS). The distribution of different adsorbent species with varying ΔW in (c) HS (d) LS. All of the data points were colored by specific cooling effects (SCE) in the single-stage.

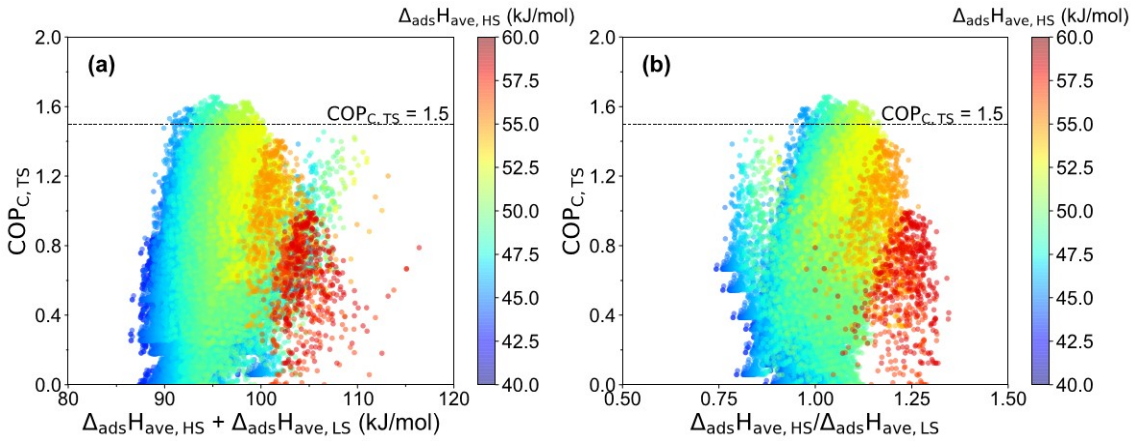

Figure S4. The relationship between the coefficient of performance for cooling (COP_C) and (a) the summation of average heat of adsorption of HS and LS ($\Delta_{ads}H_{ave,HS} + \Delta_{ads}H_{ave,LS}$), (b) the ratio of average heat of adsorption of HS and LS ($\Delta_{ads}H_{ave,HS}/\Delta_{ads}H_{ave,LS}$). The data points were colored by $\Delta_{ads}H_{ave,HS}$.

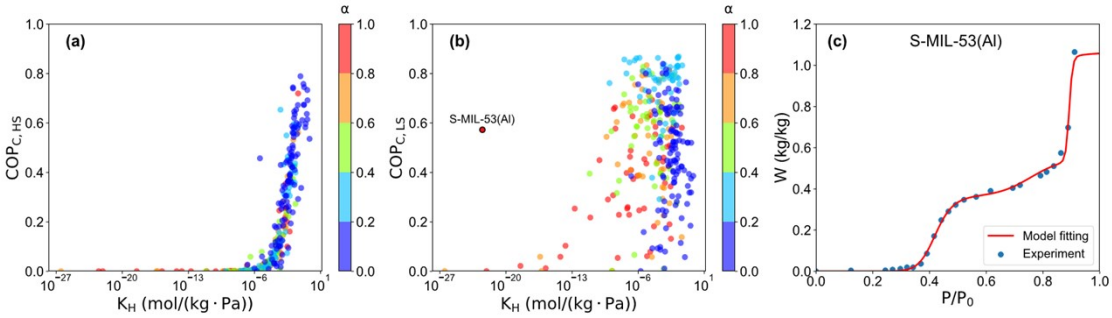

Figure S5. The relationship between the coefficient of performance for cooling (COP_C) and Henry's constant (K_H) in (a) high-temperature stage (HS) and (b) low-temperature stage (LS), and the data points were colored by step position (α) of adsorption isotherms. (c) The water adsorption isotherm of S-MIL-53(Al)[4] at 298 K was fitted by universal adsorption isotherm model (UAIM).

The positive relationship between COP_C and the K_H in single-stage, as well as the optimal range of K_H for adsorbents with high COP_C (i.e., $10^{-3} < K_{H,HS} < 10^{0}$ for $COP_{C,HS} > 0.7$, and $10^{-7} < K_{H,LS} < 10^{-1}$ for $COP_{C,LS} > 0.8$) was shown in Figure S4. Besides, the negative correlation between K_H and step position (α) was observed. Normally, the adsorption chillers (ACs) with S-MIL-53(Al)[4]/water as working pairs in LS showed low Henry's constant (K_H) and larger step position (α) ($0.8 < \alpha < 1.0$) of adsorption isotherm. However, it performed higher COP_C around 0.6 than other adsorbents with similar K_H and α, which due to its adsorption isotherms with multiple adsorption steps (Figure S4c) that results in decent working capacity at applied working conditions.

Table S7. The number of adsorbents in the different range of step position (α) at 298 K.

α	Number	Species				
		Carbon	COFs	MOFs	POPs	Zeolites
0.0-0.1	76	3	3	61	—	9
0.1-0.2	34	1	4	26	2	1
0.2-0.3	27	5	4	18	—	—

0.3-0.4	26	3	6	17	—	—
0.4-0.5	19	2	4	13	—	—
0.5-0.6	27	7	11	6	3	—
0.6-0.7	24	6	9	6	3	—
0.7-0.8	27	2	6	10	8	1
0.8-0.9	33	4	9	12	8	—
0.9-1.0	18	4	1	7	6	—
Sum	311	37	57	176	30	11

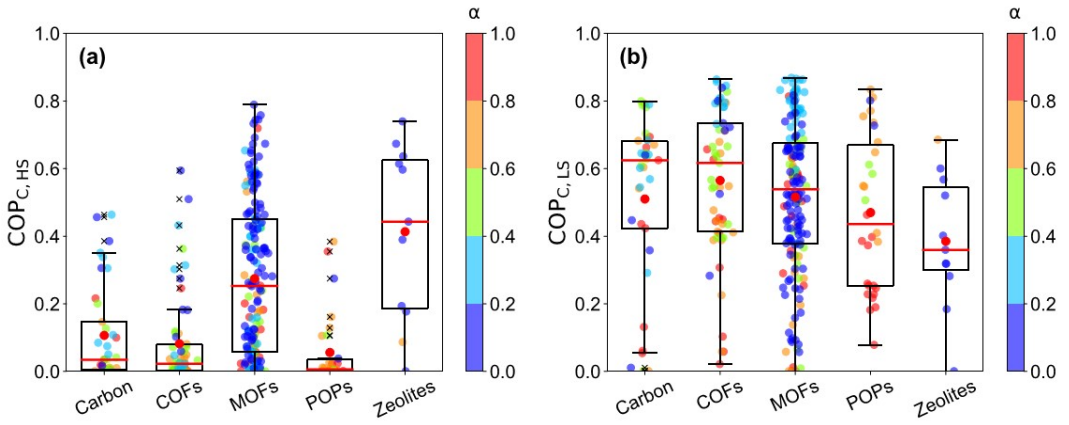

Figure S6. The distribution of different adsorbent species with varying coefficient of performance for cooling (COP_C) in (a) high-temperature stage (HS) and (b) low-temperature stage (LS), and data points were colored by step position (α) of adsorption isotherms.

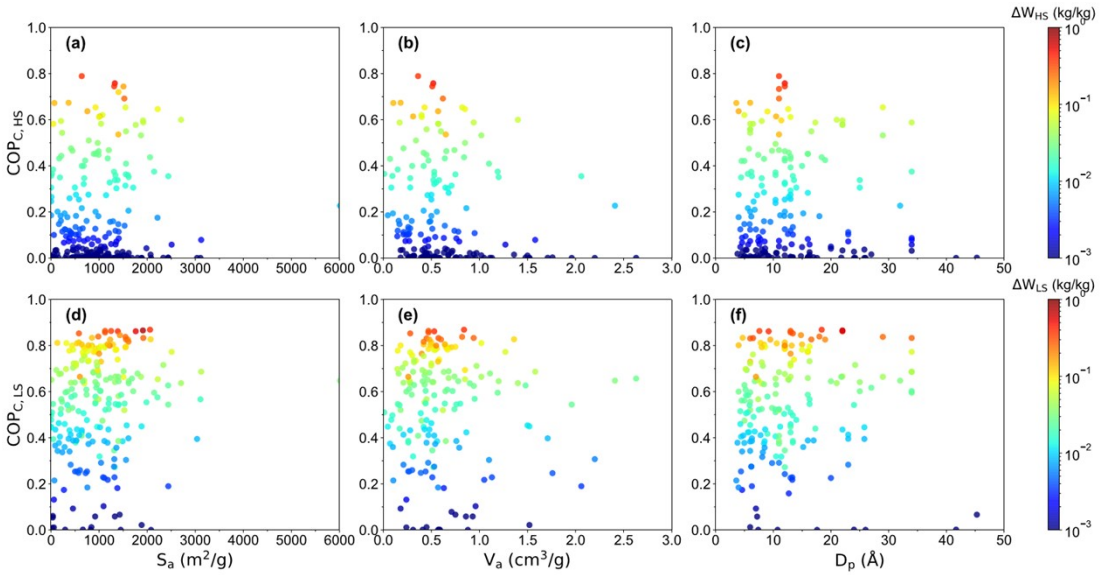

Figure S7. The relationship between coefficient of performance for cooling (COP_C) and structural characteristics (S_a is accessible surface area, V_a is available pore volume, D_p is pore size), which is colored by water working capacity (ΔW) for (a-c) high-temperature stage (HS) and (d-f) low-temperature stage(LS).

Table S8. Top 10 adsorbents with the highest $COP_{C,HS}$ in HS

No.	Adsorbents	Species	Component		S_a (m^2/g)	V_a (cm^3/g)	D_p (Å)	ΔW_{HS} (kg/kg)	$\Delta_{ads}H_{ave}$ (kJ/mol)	α	K_H (mol/(kg·Pa))	$COP_{C,HS}$	SCE_{HS} (kJ/kg)	Water stability
			Metal	Linker										
1	Ni-DOBDC [5]	MOF	Ni	DOBDC	639	0.362	11 [c1]	0.38	48.30	0.0-0.1	7.41×10^{-2}	0.789	907	No loss in ΔW over 50 ads. cycles [6]
2	Co-MOF-74(S) [7]	MOF	Co	DOBDC	1327	0.52	12 [c1]	0.49	51.48	0.0-0.1	1.53×10^{-1}	0.758	1175	37% loss in W_{max} over 1-2 ads. cycles, no loss in W_{max} over 2-5 ads. cycles [8]
3	Co-MOF-74(M) [7]	MOF	Co	DOBDC	1314	0.51	12 [c1]	0.39	51.56	0.0-0.1	1.80×10^{-1}	0.745	927	37% loss in W_{max} over 1-2 ads. cycles, no loss in W_{max} over 2-5 ads. cycles [8]
4	CuBTC [9]	MOF	Cu	BTC	1507	n.d.	n.d.	0.16	47.74	0.0-0.1	1.19×10^{-2}	0.744	389	42% loss in W_{max} after 10 ads. cycles [10]
5	Zeolite Na-A [11]	Zeolite	Na, Al, Si, O		n.d.	n.d.	n.d.	0.19	49.20	0.0-0.1	1.22×10^{-2}	0.739	453	Water stable
6	CPO-27-Ni [12]	MOF	Ni	DOBDC	n.d.	n.d.	11 [c1]	0.32	50.11	0.0-0.1	3.95×10^{-1}	0.733	768	No loss in ΔW over 50 ads. cycles [6]
7	HKUST-1-F [13]	MOF	Cu	BTC-F	1404	n.d.	n.d.	0.11	45.65	0.9-1.0	4.20×10^{-2}	0.719	265	n.d.
8	Mg-MOF-74 [14]	MOF	Mg	DOBDC	1525	0.62	11 [c1]	0.25	50.25	0.0-0.1	4.15×10^{-1}	0.691	608	49% loss in W_{max} over 1-2 ads. cycles, no loss in W_{max} over 2-5 ads. cycles [8]
9	Zn-MOF-74 (cycle 1) [15]	MOF	Zn	DOBDC	n.d.	n.d.	n.d.	0.14	49.74	0.0-0.1	1.72×10^{-1}	0.673	327	50% loss in W_{max} over 1-2 ads. cycles, no loss in W_{max} over 2-5 ads. cycles [15]
10	Na-ZSM-5 [16]	Zeolite	Na, Al, Si, O		366	0.18	6 [c1]	0.13	50.61	0.0-0.1	1.61×10^{-1}	0.673	325	Water stable

Table S9. Top 10 adsorbents with the highest $COP_{C,LS}$ in LS

No.	Adsorbents	Species	Component		S_a (m^2/g)	V_a (cm^3/g)	D_p (Å)	ΔW_{LS} (kg/kg)	$\Delta_{ads}H_{ave}$ (kJ/mol)	α	K_H (mol/(kg·Pa))	$COP_{C,LS}$	SCE_{LS} (kJ/kg)	Water stability
			Metal	Linker										
1	Zr-MOF-808 [8]	MOF	Zr	BTC	2060	0.84	18.4 [c1]	0.40	46.68	0.3-0.4	1.97×10^{-2}	0.868	951	Unstable/strong water ads. [8]
2	Co_2Cl_2(BTDD) [17]	MOF	Co	BTDD	1912	n.d.	22 [c2]	0.75	47.25	0.2-0.3	1.54×10^{-2}	0.865	1799	6.3% loss in ΔW over 30 ads. cycles [17]
3	AB-COF [18]	COF	1,3,5-triformyl benzene, hydrazine		1125	0.47	13 [c1]	0.29	46.46	0.2-0.3	1.38×10^{-6}	0.864	704	Fully reversible ΔW over 4 ads. cycles [18]
4	CAU-23 [19]	MOF	Al	TDC	1250	n.d.	7.6 [c2]	0.34	46.80	0.2-0.3	1.24×10^{-4}	0.863	825	No loss in ΔW over 5000 ads. cycles [19]

5	Ni_2Cl_2(BTDD) [17]	MOF	Ni	BTDD	1762	n.d.	22 [c2]	0.54	47.18	0.3-0.4	1.59×10^{-2}	0.862	1292	Little loss in S_{BET} after water ads. [17]
6	Zr-MOF-841 [8]	MOF	Zr	MTB	1390	0.53	9.2 [c1]	0.41	47.03	0.2-0.3	6.55×10^{-7}	0.862	975	7% loss in W_{max} after 5 ads. cycles [8]
7	Mg-CUK-1 [20]	MOF	Mg,	PDC	580	0.28	13.4 [c2]	0.29	47.04	0.2-0.3	4.19×10^{-7}	0.853	698	No loss in ΔW over 50 ads. cycles [20]
8	TpPa-1 (Karak) [21]	COF	Tp, Pa-1		1432	n.d.	14.8 [c1]	0.19	45.87	0.2-0.3	1.21×10^{-7}	0.845	459	No loss in ΔW over 4 ads. cycles [21]
9	TpPa-1 (Biswal) [22]	COF	Tp, Pa-1		984	n.d.	18 [c1]	0.25	46.89	0.1-0.2	4.15×10^{-4}	0.839	592	No loss in ΔW over 10 ads. cycles [22]
10	MIL-100(Fe) [23]	MOF	Fe	BTC	1549	0.82	29 [c2]	0.25	46.81	0.3-0.4	5.68×10^{-4}	0.837	593	No loss in ΔW over 10 ads. cycles [24]

n.d. represents "no data".

For D_p: [c1] average pore diameter, [c2] largest cavity diameter, [c3] dominant pore size obtained according to pore size distribution.

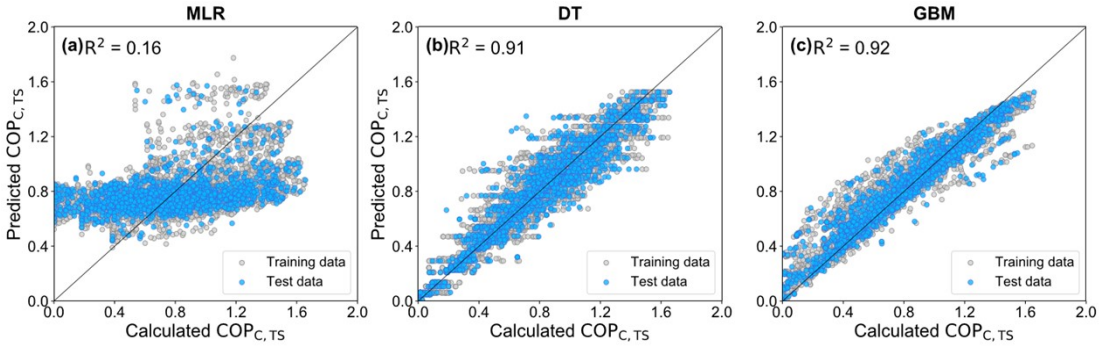

Figure S8. The coefficient of performance of the total system ($COP_{C,TS}$) is predicted by varying machine learning models (a) multiple linear regression (MLR), (b) decision tree (DT) and (c) gradient boosting machine (GBM)

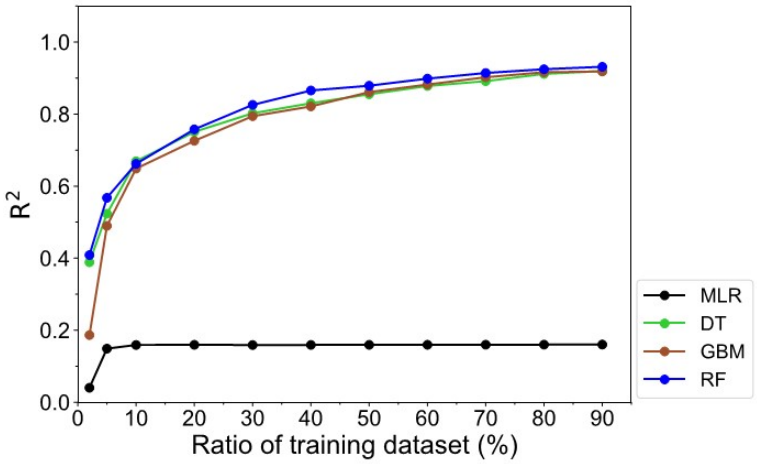

Figure S9. The R^2 for predicting COP_C using four ML models (MLR, DT, GBM and RF) under the various ratios of the training dataset

References

1. K. C. Ng, M. Burhan, M. W. Shahzad and A. B. Ismail, *Sci. Rep.*, 2017, **7**, 10634.
2. Z. Liu, W. Li, P. Z. Moghadam and S. Li, *Sustainable Energy & Fuels*, 2021, **5**, 1075-1084.
3. M. F. d. Lange, K. J. F. M. Verouden, T. J. H. Vlugt, J. Gascon and F. Kapteijn, *Chem. Rev.*, 2015, **115**, 12205-12250.
4. M. G. Goesten, J. Juan-Alcañiz, E. V. Ramos-Fernandez, K. B. Sai Sankar Gupta, E. Stavitski, H. van Bekkum, J. Gascon and F. Kapteijn, *J. Catal.*, 2011, **281**, 177-187.
5. J. Liu, Y. Wang, A. I. Benin, P. Jakubczak, R. R. Willis and M. D. LeVan, *Langmuir*, 2010, **26**, 14301-14307.
6. B. Shi, A.-D. Raya, S. Mahmoud, A. Elsayed and E. Elsayed, *Appl. Therm. Eng.*, 2016, **106**, 325-333.
7. H.-Y. Cho, D.-A. Yang, J. Kim, S.-Y. Jeong and W.-S. Ahn, *Catal. Today*, 2012, **185**, 35-40.
8. H. Furukawa, F. Gandara, Y. B. Zhang, J. Jiang, W. L. Queen, M. R. Hudson and O. M. Yaghi, *J. Am. Chem. Soc.*, 2014, **136**, 4369-4381.
9. J. Kim, S.-H. Kim, S.-T. Yang and W.-S. Ahn, *Microporous Mesoporous Mater.*, 2012, **161**, 48-55.
10. M. Wöllner, N. Klein and S. Kaskel, *Microporous Mesoporous Mater.*, 2019, **278**, 206-211.
11. S.-i. Furukawa, K. Goda, Y. Zhang and T. Nitta, *J. Chem. Eng. Jpn.*, 2004, **37**, 67-74.
12. A. Das, P. D. Southon, M. Zhao, C. J. Kepert, A. T. Harris and D. M. D'Alessandro, *Dalton Trans*, 2012, **41**, 11739-11744.
13. N. Ko, J. Hong, L. You, H. J. Park, J. K. Yang and J. Kim, *Bull. Korean Chem. Soc.*, 2015, **36**, 327-332.
14. D.-A. Yang, H.-Y. Cho, J. Kim, S.-T. Yang and W.-S. Ahn, *Energy Environ. Sci.*, 2012, **5**, 6465-6473.
15. Y. Li, X. Wang, D. Xu, J. D. Chung, M. Kaviany and B. Huang, *J. Phys. Chem. C*, 2015, **119**, 13021-13031.
16. L. N. Ho, Y. Schuurman, D. Farrusseng and B. Coasne, *J. Phys. Chem. C*, 2015, **119**, 21547-21554.
17. A. J. Rieth, S. Yang, E. N. Wang and M. Dinca, *ACS Cent. Sci.*, 2017, **3**, 668-672.
18. L. Stegbauer, M. W. Hahn, A. Jentys, G. Savasci, C. Ochsenfeld, J. A. Lercher and B. V. Lotsch, *Chem. Mater.*, 2015, **27**, 7874-7881.
19. D. Lenzen, J. Zhao, S. J. Ernst, M. Wahiduzzaman, A. Ken Inge, D. Frohlich, H. Xu, H. J. Bart, C. Janiak, S. Henninger, G. Maurin, X. Zou and N. Stock, *Nat. Commun.*, 2019, **10**, 3025.
20. J. S. Lee, J. W. Yoon, P. G. M. Mileo, K. H. Cho, J. Park, K. Kim, H. Kim, M. F. de Lange, F. Kapteijn, G. Maurin, S. M. Humphrey and J. S. Chang, *ACS Appl. Mater. Interfaces*, 2019, **11**, 25778-25789.
21. S. Karak, S. Kandambeth, B. P. Biswal, H. S. Sasmal, S. Kumar, P. Pachfule and R. Banerjee, *J. Am. Chem. Soc.*, 2017, **139**, 1856-1862.
22. B. P. Biswal, S. Kandambeth, S. Chandra, D. B. Shinde, S. Bera, S. Karak, B. Garai, U. K. Kharul and R. Banerjee, *J. Mater. Chem. A*, 2015, **3**, 23664-23669.
23. P. Küsgens, M. Rose, I. Senkovska, H. Fröde, A. Henschel, S. Siegle and S. Kaskel, *Microporous Mesoporous Mater.*, 2009, **120**, 325-330.
24. Y. K. Seo, J. W. Yoon, J. S. Lee, Y. K. Hwang, C. H. Jun, J. S. Chang, S. Wuttke, P. Bazin, A. Vimont and M. Daturi, *Adv. Mater.*, 2012, **24**, 806-810.